Published in "Journal of Physics B: Atomic, Molecular and Optical Physics
46(4): 045203 , 2013"
which should be cited to refer to this work.

Electron impact excitation of methane: determination of appearance energies for dissociation products

M Danko[1], J Orszagh[1], M Ďurian[1], J Kočišek[1], M Daxner[2], S Zöttl[2], J B Maljković[3], J Fedor[4], P Scheier[2], S Denifl[2,5] and Š Matejčík[1,5]

[1] Department of Experimental Physics, Faculty of Mathematics, Physics and Informatics, Comenius University, Mlynská dolina, 84248 Bratislava, Slovakia
[2] Institute for Ion Physics and Applied Physics, Association Euroatom ÖAW, University of Innsbruck, Technikerstrasse 25, A-6020 Innsbruck, Austria
[3] Laboratory for Atomic Collision Processes, Institute of Physics, University of Belgrade, Pregrevica 118, 11080 Belgrade, Serbia
[4] Department of Chemistry, University of Fribourg, Chemin du Musée 9, CH-1700 Fribourg, Switzerland

E-mail: matejcik@fmph.uniba.sk and Stephan.Denifl@uibk.ac.at

Abstract
In this work, we present an experimental study of dissociative excitation of CH_4 utilizing a crossed electron molecular beam experiment. Methane was excited by nearly monochromatic electrons generated by a trochoidal electron monochromator. The dissociative products were identified on the basis of the emission spectra in the ultraviolet–visible (UV/VIS) spectral range. The excitation functions were recorded as the function of the electron energy for different emission bands of the fragments (Balmer series for H: $n = 3{,}4 \ldots 9 \rightarrow 2$, and moreover, CH: $A^2\Delta \rightarrow X^2\Pi$, CH: $B^2\Sigma^- \rightarrow X^2\Pi$, CH: $C^2\Sigma^+ \rightarrow X^2\Pi$, CH^+: $B^1\Delta \rightarrow A^1\Pi$, and CI: $2p3s\ ^1P^o_1 \rightarrow 2p^2\ ^1S_0$). From the experimental data we have determined the threshold energies for excitation of particular fragments. Present experimental results indicate that the threshold energies for some dissociative excitation channels could be lower by ∼1–2 eV in comparison to earlier studies and indicate that different dissociative processes may be operative at the threshold than assumed in the former studies.

Online supplementary data available

Introduction

Collisions of electrons with methane play an important role in several areas of physics and chemistry [1]. This arises from the fact that methane is present in planetary atmospheres (like, for example, Earth, Jupiter or Titan) [2–7] as well as in the interstellar medium [8]. Moreover, it is also of relevance in the divertor region of thermonuclear fusion plasmas [9] and in technological low temperature plasmas [10]. Radiative and collisional processes in the plasma edge region play a considerable role for controlling the dynamics of a plasma and hence its stability. It needs to be kept in mind, however, that simple hydrocarbon molecules like methane are released by chemical erosion of the plasma vessel due to plasma–wall interactions. Although efforts are made to replace carbon-based composites with other materials like tungsten or beryllium, divertors still consist preferentially of carbon due to the high heat load [9]. Thus, data on electron–hydrocarbon collisions are required which are important factors for the simulations of the transport of impurities and their chemistry in the scrape-off layer plasma. It should be noted that for small hydrocarbons (including methane) collisional data have

[5] Authors to whom any correspondence should be addressed.

been compiled in the HYDKIN database [11, 12], which includes (dissociative) electron ionization cross sections, recombination cross sections as well as dissociative electron excitation cross sections.

Due to the broad field of applications for studies on methane an extended number of previous experimental investigations on electron ionization (see [13, 14]), electron attachment [15, 16] and dissociative electron impact excitation can be found in the literature for this molecule [17–20]. Emission spectra for electron projectiles [11–14] as well as for photo-excitation [21–23] were reported. In contrast to photo-excitation, electron impact implies also optically forbidden excited states and monitors their subsequent decay to lower states. Pang *et al* investigated electron impact emission cross sections for CH_4 and C_2H_2 in the VUV region from 40 to 200 nm [17]. Three studies are most related to the present study since electrons were used as projectiles and fluorescence signals in the VIS/UV range were recorded. Aarts *et al* [18] reported absolute emission cross sections for Balmer H_β and CH ($A^2\Delta \rightarrow X^2\Pi$) radiation between 20 eV and 5 keV. Moreover, they reported the threshold energies for these transitions and additionally for H_α and H_γ. Donohue *et al* [19] measured photon emission from fragments formed upon electron impact with methane, ethylene and methanol in the spectral range between 180 nm and 500 nm. They reported a larger number of transitions compared to Aarts *et al* including fluorescence signal from ionic CH^+ and atomic carbon fragments and determined threshold values as well. A more recent fluorescence study on methane using electrons as projectiles was carried out by Motohashi *et al* [20] who determined absolute emission cross sections for several transitions of hydrogen (Lyman α-ε and Balmer α-ε series), CH ($A^2\Delta \rightarrow X^2\Pi$) and C ($2p3s \rightarrow 2p^2$ and $2s2p^3 \rightarrow 2s^22p^2$, respectively). They investigated the electron energy range from threshold up to 1 keV and determined the appearance energies for some of the transitions mentioned. All references on electron impact of methane [17–20] investigated also the high energy range in which Fano plots reveal the optical activity of the investigated transition. It turned out that most fragments formed in electron impact excitation are formed from the ground state of CH_4 via optically forbidden states. We note that very recently also coincidence techniques were used to measure the electron energy loss spectra of 80 eV electrons in collisions with CH_4 tagged with Lyman alpha emission [24, 25].

In the present study, we investigated dissociative electron excitation of methane utilizing a monochromatized electron beam (generated by a trochoidal electron monochromator—TEM) and a detection system to monitor the fluorescence of (electronically) excited species. We recorded the emission spectrum in the spectral region from 185 to 710 nm at the electron energy of 50 eV. Subsequently, we determined the electron energy dependence for the transitions observed and derived thresholds for the corresponding transitions. For the majority of the dissociative processes, we found that the present values of the threshold energies are considerably shifted to lower values compared to previous studies. For example, in the case of the Balmer transition H(3–2) the present value is found 1.6 eV below the earlier onset [20]. We believe that the main reason for this observation is the improved sensitivity and high signal-to-noise ratio of the present experimental system in comparison to earlier systems, as well as improved resolution in the electron energy calibration due to utilization of the electron monochromator.

Experimental details

Electron impact excitation of methane (CH_4) was studied using a recently developed crossed beam apparatus in Bratislava [26]. A detailed schematic view of the apparatus is presented in figure 1. In short, electrons thermally emitted from a commercial tungsten hairpin filament (Agar Scientic A054) were monochromatized using a trochoidal electron monochromator (TEM) [27] which employs a crossed electric and magnetic field in the dispersion region. A magnetic field of 5×10^{-3} T was used, aligned in the direction of the electron beam. For the present measurements, due to relatively low cross sections for the processes studied, the electron energy resolution of the TEM was set to 300 meV full width at half maximum (FWHM) in favour of a higher electron current (typically ~750 nA). The resolution of the electron beam was determined using the retarding potential method [28]. The electron current was monitored during the experiment using picoamperemeter Keithley 6485 and the data were recorded as a function wavelength (in the case of optical spectra) or as a function of the acceleration voltage (in the case of the energy scans). The variations of the electron current during the measurements of the optical spectra were less than 5%. In the case of electron energy scans the electron current as a function of the acceleration voltage was flat in the measured energy range with statistical fluctuations less than 10%.

The electron beam was perpendicularly crossed with an effusive beam of CH_4 molecules in the interaction zone of the TEM. The gas (from Linde Gas; purity of 99.98%) was introduced by a capillary (0.5 mm diameter and 10 mm length) connected to an external gas inlet by a leak valve. The absolute pressure inside the capillary was measured by a capacitive pressure gauge (Pfeiffer Vacuum CMR 362) and the pressure inside the capillary was kept constant during the experiments. The typical working pressure inside the vacuum chamber was 1×10^{-4} mbar as measured by ionization gauge (Pfeiffer Vacuum PBR 260), which was switched off during the measurements. The background pressure of the vacuum system without gas introduction was better than 5×10^{-8} mbar. The photons emitted from the excited species (90° in reference to the electron and molecular beam and within the 26° acceptance angle) were transferred by optical lens (bi-convex, $f = 51$ mm, UV fused silica) through an MgF_2 vacuum window out of the vacuum and focused into the entrance of a Czerny–Turner optical monochromator (1/4 m, Cornerstone 260, Newport, using 1200/mm grid in the first order) by additional lens (by plano-convex $f = 150$ mm, UV fused silica). In order to increase the signal intensity we have used an additional spherical mirror with the focus in the centre of the interaction zone. We did not use any method to determine the polarization of the emitted light in this experiment. The width

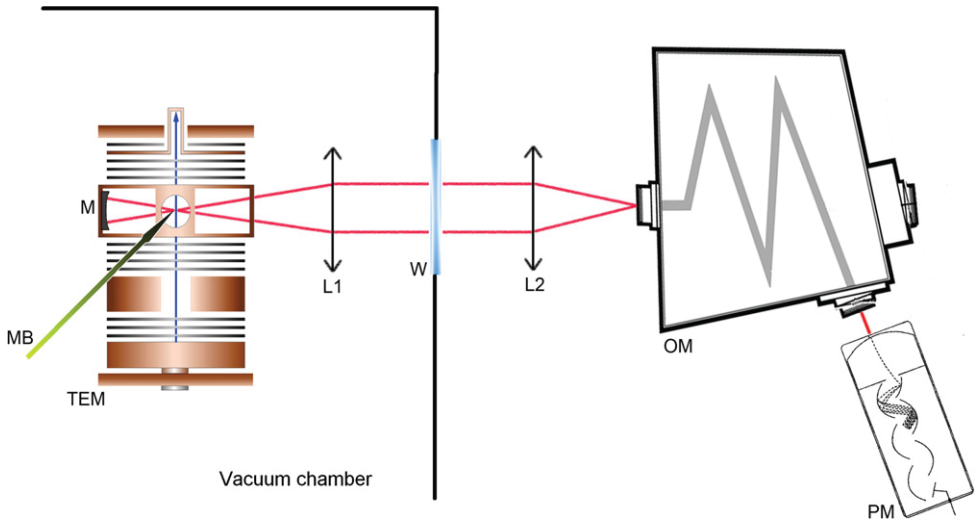

Figure 1. Schematic view of the experimental setup. TEM: trochoidal electron monochromator, MB: molecular beam, M: spherical mirror, L1, L2: fused silica lenses, W: MgF_2 window, OM: optical monochromator, PM: photomultiplier.

of the slit of the optical monochromator was set to 200 μm in order to achieve optimum sensitivity with sustaining sufficient resolution (resolution of 0.8 nm FWHM as measured at 588 nm Ar line). Higher resolution spectra have been measured with a 70 μm slit (resolution 0.3 nm FWHM as measured at the same line). The photons were detected by a Hamamatsu H4220P photomultiplier which was thermoelectrically cooled to -25 °C. The photomultiplier is sensitive in the spectral UV/VIS region between 185 and 710 nm.

In order to reduce the black-body radiation caused by the filament of the electron monochromator, the filament was located in specially designed electrodes and the surfaces of the electrodes and the inner walls of the vacuum system were covered with colloidal graphite. This considerably reduced the intensity of the background radiation so that in the present experiment the fluorescence signal was not superimposed by the background radiation from the hot filament.

We calibrated the electron energy scale by measuring the emission cross section of the (0,0) band of the second positive system of N_2 ($C^3\Pi_u \rightarrow B^3\Pi_g$) at 337 nm [26, 29] and the He I ($1s2p\ ^3P^o_{1,2}$–$1s4d\ ^3D_{1,2,3}$) 447.14 nm emission line [30]. The N_2 ($C^3\Pi_u \rightarrow B^3\Pi_g$) (0,0) cross section exhibits a pronounced peak at 14.1 eV. The cross section for the He I ($1s2p\ ^3P^o_{1,2}$–$1s4d\ ^3D_{1,2,3}$) transition exhibits a step at 23.736 eV [30]. The electron energy scale calibration was performed in the premixed mixture of CH_4:N_2:He 1:1:1 (established by absolute pressure measurement utilizing the capacitance gauge) in order to prevent the problems with different charging of the electrodes in different gases. Figure 2 shows the corresponding excitation functions for the N_2 ($C^3\Pi_u \rightarrow B^3\Pi_g$) (0,0), He I ($1s2p\ ^3P^o_{1,2}$–$1s4d\ ^3D_{1,2,3}$) and CH($A^2\Delta \rightarrow X^2\Pi$) (0,0) bands measured under the same experimental conditions. The excitation functions of N_2 and He were then used to calibrate the electron energy scale. The agreement between energy scales calibrated by N_2 and He was better than 0.015 eV. In addition, the He line has a stepwise cross section, where from the first derivative the same beam resolution was obtained as with the retarding potential method.

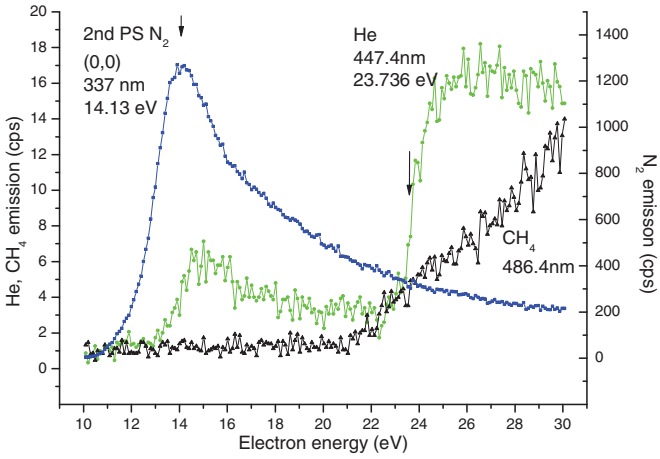

Figure 2. Excitation function of the (0,0) band of the second positive system of N_2 ($C^3\Pi_u \rightarrow B^3\Pi_g$) at 337 nm recorded as a function of the electron energy and in comparison with the CH($A^2\Delta \rightarrow X^2\Pi$) (0,0) band and cross section for the He I ($1s2p\ ^3P^o_{1,2}$–$1s4d\ ^3D_{1,2,3}$) transition, measured at the same experimental conditions. The data presented are raw data without any background subtraction or data manipulation. The arrows indicate the energy of the maximum in the emission cross section for (0,0) transition of the second positive system N_2 and the threshold for the excitation of the He excited state. The photon yield at 447.4 nm below the He onset arises from the N_2 ($C^3\Pi_u \rightarrow B^3\Pi_g$) (6,8) transition.

Two different measurement modes were used in the present study, (i) fluorescence spectra were recorded at fixed electron energies and (ii) the electron energy dependence of a specific transition was measured by setting the optical monochromator to transmit the corresponding wavelength. Apparent thresholds in the electron energy scans were deduced utilizing a fitting routine based on an exponential power law [14]. The finite electron energy resolution was also taken into account. The energy uncertainty was deduced by the fitting procedure, as the fitting procedure includes the electron energy distribution function. If the data are of good quality (the statistical scatter data are low in comparison to the real

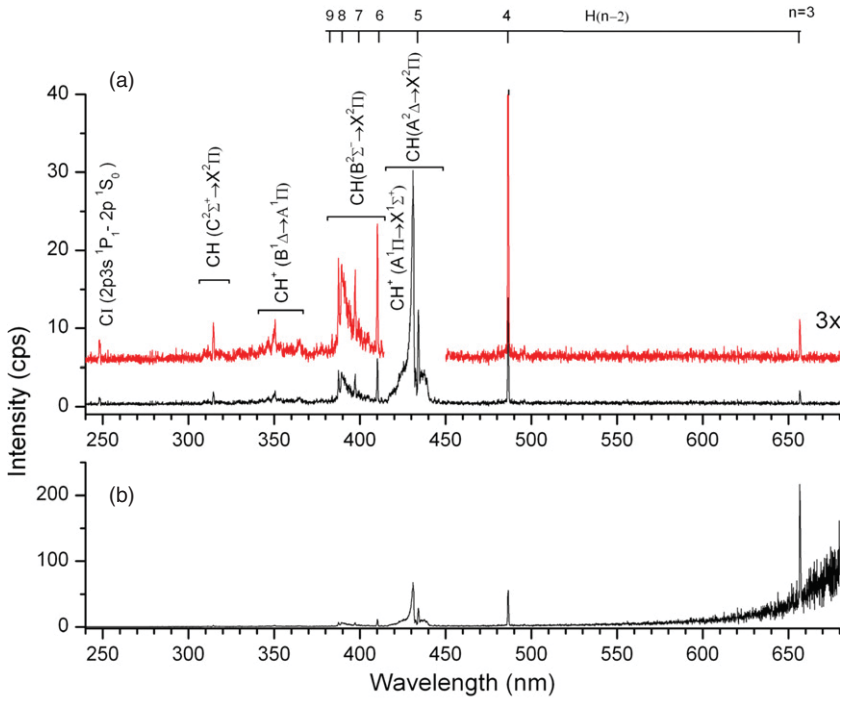

Figure 3. Emission spectrum of electronically excited species upon electron excitation (electron energy = 50 eV, optical monochromator slit 200 μm) of CH_4. (a) Uncorrected spectrum, (b) spectrum corrected for the spectral sensitivity of the optical system.

structures in the data), it is possible to achieve uncertainties in the threshold energies better than the energy resolution of the electron beam (i.e., below 0.3 eV).

Results and discussion

Figure 3 shows the emission spectrum of electronically excited species upon electron excitation of CH_4. The spectrum was recorded at the initial electron energy of 50 eV covering the spectral range between 240 and 680 nm. In the course of our study on electron excitation of methane, we observed emission signal (with photon frequency ν_{em}) from several electronically excited fragments within the spectral range of our optical monochromator:

$$e^- + CH_4 \rightarrow H(n = 3-9) + \ldots \rightarrow H(n = 2) + h\nu_{em} \quad (1)$$

$$\rightarrow CH(A^2\Delta) + \ldots \rightarrow CH\left(X^2\Pi\right) + h\nu_{em} \quad (2)$$

$$\rightarrow CH(B^2\Sigma^-) + \ldots \rightarrow CH\left(X^2\Pi\right) + h\nu_{em} \quad (3)$$

$$\rightarrow CH(C^2\Sigma^+) + \ldots \rightarrow CH\left(X^2\Pi\right) + h\nu_{em} \quad (4)$$

$$\rightarrow CH^+(B^1\Delta) + \ldots \rightarrow CH^+\left(A^1\Pi\right) + h\nu_{em} \quad (5)$$

$$\rightarrow CI(3s^1P^o) + \ldots \rightarrow CI(2p^2\,{}^1S) + h\nu_{em}. \quad (6)$$

In the emission spectrum, we also detected some additional weak bands such as the Douglas–Herzberg system CH^+(A-X) at ~422 nm. However, due to the overlap with the stronger CH(A-X) band, we were not able to separate this band in the present experiment for measurements of its excitation function. For the other atomic lines and molecular bands (1)–(6), we recorded photon yields as a function of the initial electron energy. We evaluated the curves and determined threshold energies for dissociative excitation channels.

Fluorescence spectrum

The electronic ground state of methane in T_d symmetry is $^1A_1$ $(1a_1)^2(2a_1)^2(1t_2)^6$ [31]. In agreement with all previous studies on electronic excitation of methane, photon emission from excited states of the methane molecule was not detected. Hence, the electronically excited states of methane are prone to dissociation into fragments, which are identified from the fluorescence spectrum shown in figure 3. The UV/VIS fluorescence spectrum is rich in atomic lines and molecular bands; the Balmer lines are easily identified in the spectrum as well as the emission bands of the CH($A^2\Delta \rightarrow X^2\Pi$), CH($B^2\Sigma^- \rightarrow X^2\Pi$), CH($C^2\Sigma^+ \rightarrow X^2\Pi$). A third neutral fragment observed is atomic carbon CI($2p3s\ ^1P^o_1 \rightarrow 2p^2\ ^1S_0$) at 247.9 nm. Besides the neutral species, we are able to detect weak CH^+ emission bands like the Douglas–Herzberg system $CH^+(A^1\Pi \rightarrow X^1\Sigma^+)$, $CH^+(B^1\Delta \rightarrow X^1\Sigma^+)$ as well as $CH^+(B^1\Delta \rightarrow A^1\Pi)$ transition.

Balmer series – H($n \geqslant 3 \rightarrow 2$). We focus now on the Balmer hydrogen series in methane. We were able to detect transitions as high as $n = 9$ H_η (9–2; 383.7 nm). We also observed a broad line at ~364 nm, where the Rydberg states of H are overlapped with CH($B^2\Sigma \rightarrow X^2\Pi$)(1,0). We tried to resolve this part of spectra and to obtain excitation functions for $n > 9$, however,

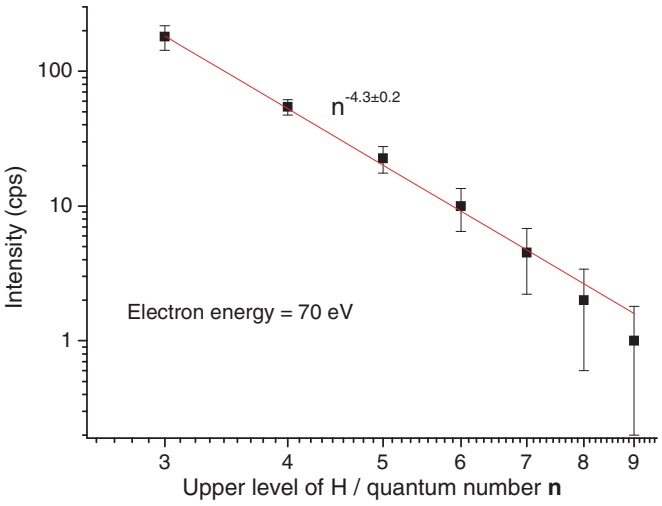

Figure 4. Double logarithmic plot of the photon yield of the Balmer lines (squares) versus the excitation state n. The best fit following an $n^{-4.3 \pm 0.2}$ dependence is shown as a solid line (see the text). The intensities of the lines were corrected for spectral response of the system and derived from figure 3(b).

due to low intensity (high noise) and limited resolution of the optical monochromator, we did not succeed.

We note that in [32] absolute emission cross sections of the Balmer series H(3–2) up to H(11–2) for 100 eV electrons impacting on methane were reported. The cross section scales strongly down with decreasing wavelength (for example, H(3– 2)/H($n \rightarrow 2$) = 556)). It was suggested theoretically by Hartree that the intensities of atomic spectral lines of a given series are proportional to n^{-3} [32] and this dependence was expected as well for excitation cross sections of atoms and as well for molecules in high Rydberg states. Möhlmann and de Heer detected for several molecules (including CH_4) that the intensities of Balmer lines follow n^{-5} dependence [32]. The deviation from the n^{-3} law was explained by contribution of autoionization states. They assumed that the high lying Rydberg states of the parent molecules are precursor states for the production of excited hydrogen. These Rydberg states are highly vibrationally excited (= super-excited states) [33] and lie energetically in the ionization continuum. Hence, the dissociative excitation is in competition with autoionization, which has higher probability the larger the n is. Motohashi *et al* observed in their electron impact excitation experiments with methane an exponent of 4.5 $\pm$ 0.2 for the Balmer series [20] in agreement with [32]. In contrast, the exponential factors of the Balmer hydrogen series for dissociation of larger molecules like furan, tetrahydrofuran and isoxacole [34–36] yielded values much closer to the theoretical value (between 3.2 and 3.74). The dependence of the Balmer line intensities on n as obtained in the present experiment is presented in figure 4. The Balmer line intensities I are given in photon counts per seconds (cps) corrected for spectral response of the apparatus. As the spectrum was measured at constant electron current, the intensities are proportional to the excitation cross section. The systematic uncertainty of this cross section is wavelength dependent and we estimate an uncertainty of 20% in the wavelength range below 300 nm, 5–10% in the region between 300 and 500 nm and 20% above 500 nm. The value of the exponent of 4.3 $\pm$ 0.2 derived here using least-squares method fitting is in good agreement with the values previously determined by Möhlmann and de Heer [32] as well as Motohashi *et al* [20].

CH emission. As mentioned above the highest fluorescence signal from an excited molecular fragment is observed for CH. In the present experiment, we can monitor three bands, $A^2\Delta \rightarrow X^2\Pi$ (0,0) (430.9 nm), $B^2\Sigma^- \rightarrow X^2\Pi$ (0,0) (387.5 nm) and $C^2\Sigma^+ \rightarrow X^2\Pi$ (0,0) (314.5 nm). The latter transition was reported in the previous electron impact excitation studies by Donohue *et al* [19] only. A closer look into the fluorescence spectrum (see figure 3) reveals clearly ro-vibrational structure of these CH bands. For example, figure 5(a) shows the CH(A-X) system between 415 and 445 nm in detail recorded at higher resolution (70 μm slit of the optical monochromator). The simulation of this spectrum was carried out utilizing the LIFBASE program [37]. The photon yield in this range can be mainly ascribed to the $A^2\Delta \rightarrow X^2\Pi$ including R, Q and P branches of 0–0, 1–1 and 2–2 bands [38], superposed with the H(5–2) line at 434.2 nm. Moreover, we were able to recognize in this spectral range of the measured spectrum weak structures resulting from the Douglas–Herzberg system $CH^+(A^2\Delta \rightarrow X^2\Pi)$ at ~422 nm and $CH(B^2\Sigma^- \rightarrow X^2\Pi)$ (0,1) above 435 nm as well. Ro-vibrational structures were observed between 387 and 407 nm due to bands of $CH(B^2\Sigma^- \rightarrow X^2\Pi)$ (0–0) transition (figure 5(b)) and between 362 and 367 nm due to branches of the $CH(B^2\Sigma^- \rightarrow X^2\Pi)$ (1–0) band [21]. The line at 386.2 nm in figure 4(b) could be assigned to the second order of the CI ($2s^22p^2\ ^1D_2 \rightarrow 2s^22p3s\ ^1P^\circ_1$) line at 193.1 nm. This assignment is supported by the reduced width of this atomic line in comparison to the first order line, which we detected as well, however, is not depicted in the spectrum shown in figure 3.

In view of the ro-vibrational analysis of the emission spectra of CH_4, we mention the study by Kong *et al* [21] who used intense femtosecond laser pulses to excite and dissociate CH_4 and measure fluorescence of excited fragments formed. Their fluorescence spectrum showed pronounced ro-vibrational emission spectra of the CH radical which indicated highly energized fragmentation products (termed as 'molecular explosion' in [21]). They deduced ro-vibrational temperatures from the ro-vibrational distribution representing a Boltzmann distribution and obtained temperatures between 1100 $\pm$ 500 K ($C^2\Sigma^+$ state) and 2800 $\pm$ 400 K ($A^2\Delta$). Ito *et al* [38] studied the internal energy distribution of the CH $A^2\Delta$ state formed by electron impact dissociation of methyl halides and observed a vibrational temperature of 3300 $\pm$ 400. It is also stated in [38] that similar temperatures can be obtained for small hydrocarbons like methane, acetylene and ethylene, which, however, was not confirmed later by Tokeshi *et al* using electron impact [39] and fast argon ion impact [40].

From the analysis of the present fluorescence spectrum, we may also quantitatively estimate the rotational and vibrational distributions of the CH excited states after electron impact. As mentioned above, we performed the simulation of the emission spectra utilizing the program LIFBASE [37].

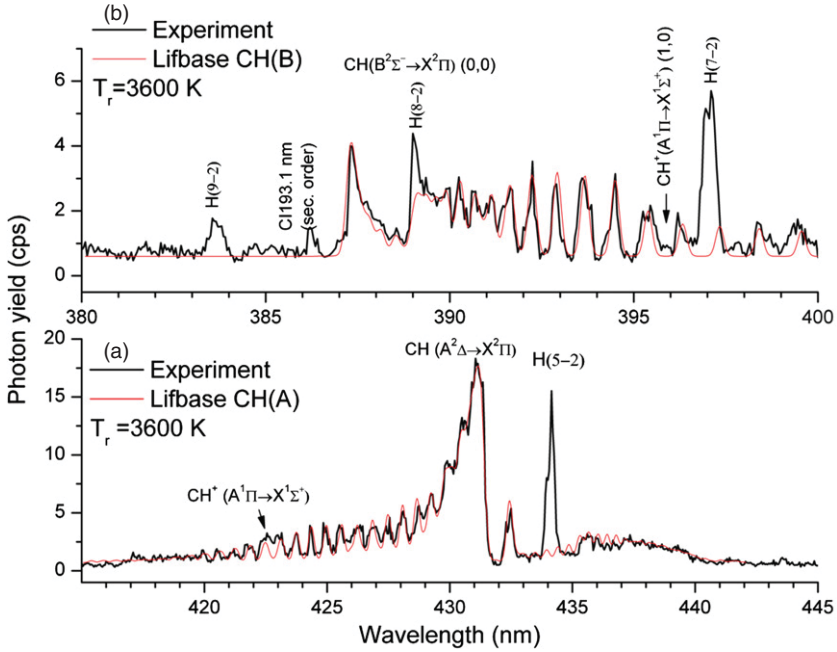

Figure 5. High-resolution emission spectra (electron energy = 50 eV, optical monochromator slit 70 μm) between (a) 415 and 445 nm and (b) 380 and 400 nm. The experimental data are compared with calculated intensities using the LIFBASE program (see the text).

The best agreement between simulated and measured spectra was achieved (eyeball fitting) for CH(A) (figure 5(a)) using rotational temperature $T_r = 3600 \pm 500$ K. In the simulation we have used the Voigt profile for the apparatus function, 0.25 nm FWHM (with 5% Lorentzian contribution). The vibrational distribution of the CH(A) was non-thermal with $\nu = 0$ 55.26%, $\nu = 1$ 18.22%, $\nu = 2$ 15.64% and $\nu = 3$ 10.87%. In the case of the CH(B), the simulated spectrum in figure 5(b) was generated for $\nu = 0$ and 100% population of this vibrational state and the rotational distribution was as well characterized by the $T_r = 3600 \pm 500$ K. We believe that the concept of temperature in the case of the fluorescence spectra may not be correct since the excitation–dissociation process of one molecule does not correspond to a thermodynamic equilibrium situation (Boltzmann distribution). Instead the amount of ro-vibrational excitation rather corresponds to the transition probabilities between the various states, i.e. the temperature depends on the Franck–Condon factors for the various transitions.

CH^+ emission. The present fluorescence spectrum also shows emission from ionic species which can be ascribed to CH^+. Fluorescence of the latter ion was studied in detail previously [41], investigating the C^+-H_2 collision system. Donohue *et al* [19] reported bands corresponding to $CH^+(B^1\Delta \rightarrow A^1\Pi)$ (350.3 nm), $CH^+(b^3\Sigma \rightarrow a^3\Pi)$ (348.7 nm) and $CH^+(A^1\Pi \rightarrow X^1\Sigma^+)$ (422.6 nm) upon electron impact excitation of methane. The intensity of other vibrational transitions of the Douglas–Herzberg system ($A^1\Pi \rightarrow X^1\Sigma^+$) of the CH^+ ion [42], ((1—0) at 395.7 nm and (2–0) at 374.5 nm) are at the detection limit of the present technique, which is mainly limited by the low electron current and the dark count rate of the photomultiplier. In contrast to the $CH^+(B^1\Delta \rightarrow A^1\Pi)$ and $CH^+(A^1\Pi \rightarrow X^1\Sigma^+)$, we do not see a clear indication of the $b^3\Sigma \rightarrow a^3\Pi$ transition: no peak is visible at 348.8 nm corresponding to the (0–0) band and moreover, we also do not observe the (1–1) band at 337 nm present in data of Harris *et al* [41]. In favour of an improved energy resolution, the present experiments were carried out with electron current several orders of magnitude lower in comparison to experiments with a simple electron gun. This is the most probable reason why some spectral features were not detected here, even when we increased the data acquisition time.

Threshold energies

In figure 6, we present as an example a selection of excitation functions for several emission lines and bands as a function of the electron energy. More excitation functions can be found in the supplementary material, available at stacks.iop.org/JPhysB/46/045203/mmedia. In tables 1 and 2 we list the corresponding thresholds for the Balmer hydrogen series and (hydro)carbon fragments, respectively. The present values are compared in these tables with threshold values reported in previous studies. For a few transitions investigated here (H_ε(7–2), H_ζ(8–2), H_η(9–2), $CH(B^2\Sigma^- \rightarrow X^2\Pi)$) no threshold values for electron impact can be found in the literature to the best of our knowledge. Threshold energies for a transition also give information on the molecular state involved. Bettega *et al* [43] calculated the lowest lying excited states of methane which are $^3T_2$ states. The lowest state was found to be at 10.84 eV (in very good agreement with Winstead *et al* [44] and Gil *et al* [45]). All electronically excited states of methane are dissociative [44]. For example, it was proposed that all states below 13 eV will lead to the production of the neutral CH_3 radical with a threshold energy of 7.5 ± 0.3 eV as determined by post-ionization of the fragment formed after dissociative excitation of CH_4 [46].

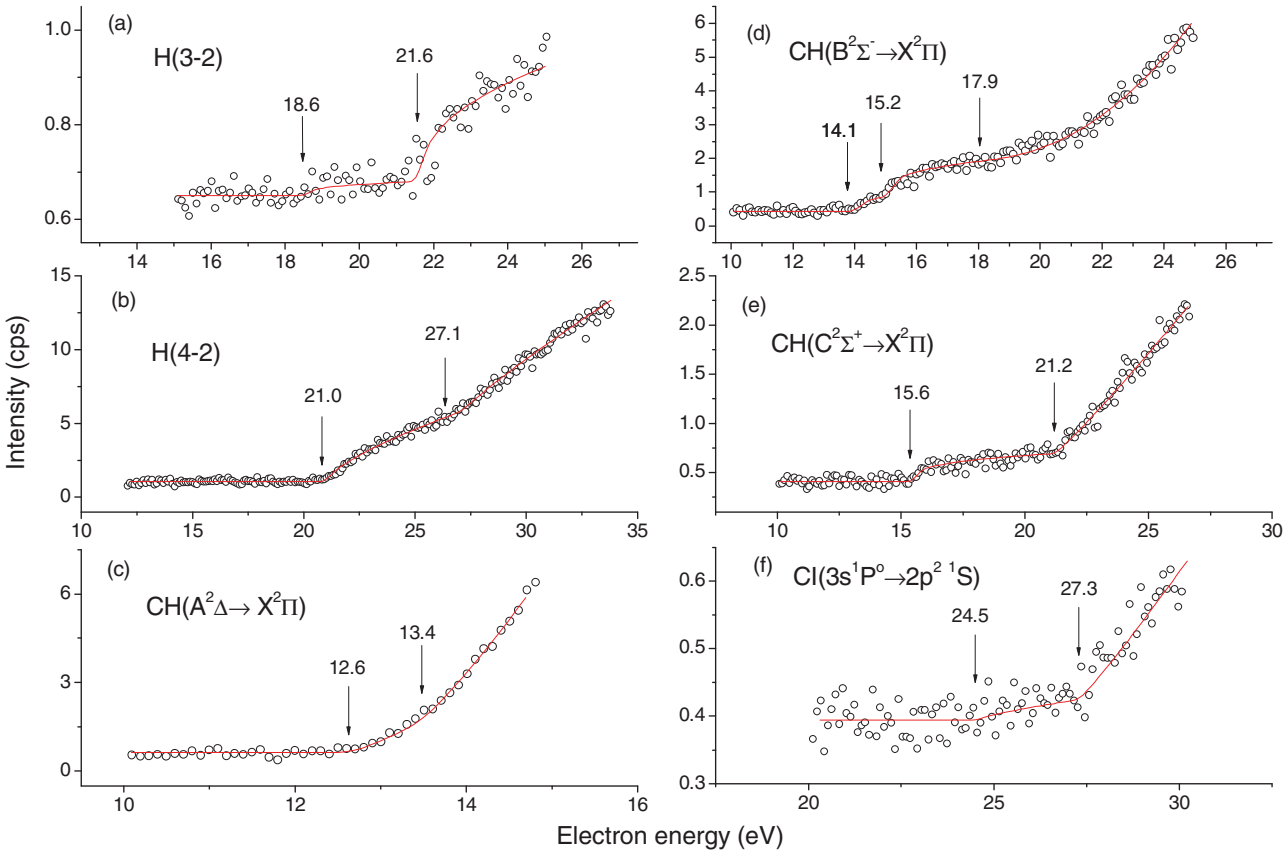

Figure 6. Photon yield of selected transitions measured as a function of the initial electron energy. Observed thresholds obtained using the fitting method in the measured energy range are indicated by arrows.

Table 1. Threshold energies for the Balmer series (H($n \geqslant 3 \rightarrow 2$)) obtained in the present experiment. The present values are compared with values calculated for selected reaction channels from thermochemical data [47] and with earlier experimental values.

				Threshold energy (eV)				
	Fragment	Transition	Observed wavelength (nm)	Calc.	Present	[20]	[18]	[19]
1a	$CH_3(X) + H^*$	H(3–2)	656.9	16.65	18.6 ± 0.2	20.2	21.9 ± 0.5	
1b	$CH(X) + H_2 + H^*$			21.23				
1c	$CH_2(X) + H + H^*$			21.40	21.6 ± 0.4	26.2 36		
2a	$CH_3(X) + H^*$	H(4–2)	486.4	17.30	21.0 ± 0.2	20.5	21.8 ± 0.5	22
2b	$CH(X) + H_2 + H^*$			21.88				
2c	$CH_2(X) + H + H^*$			22.05	27.10 ± 0.4	26.3		27.4 36.5
3a	$CH_3(X) + H^*$	H(5–2)	434.2	17.61	21.5 ± 0.3	20.7	22.3 ± 0.5	22.6
3b	$CH(X) + H_2 + H^*$			22.19				
3c	$CH_2(X) + H + H^*$			22.36	26.7 ± 0.4	28		28
4a	$CH_3(X) + H^*$	H(6–2)	410.1	17.77	21.9 ± 0.3	21		
4b	$CH(X) + H_2 + H^*$			22.35				
4c	$CH_2(X) + H + H^*$			22.52	25.4 ± 0.5	27		
5	$CH_3(X) + H^*$	H(7–2)	397.1	17.868	20.6 ± 0.2			
	$CH(X) + H_2 + H^*$			22.453	28.3 ± 0.4			
	$CH_2(X) + H + H^*$			22.622				
6	$CH_3(X) + H^*$	H(8–2)	389.2	17.933	21.8 ± 0.3			
	$CH(X) + H_2 + H^*$			22.518				
	$CH_2(X) + H + H^*$			22.687				
7	$CH_3(X) + H^*$	H(9–2)	383.7	17.978	22.3 ± 0.3			
	$CH(X) + H_2 + H^*$			22.563	29.1 ± 0.4			
	$CH_2(X) + H + H^*$			22.732				

Table 2. Threshold energies for CH, CH^+ and CI emission obtained in the present experiment. The present values are compared with values calculated for selected reaction channels from thermochemical data [47] and earlier experimental values.

				Threshold energy (eV)				
	Fragment	Transition	Observed wavelength (nm)	Calc.	Present	[20]	[18]	[19]
8a	$CH(A) + H + H_2$	$A^2\Delta \rightarrow X^2\Pi$	430.9	12.01	12.6 ± 0.2			
8b	$CH(A) + 3H$				13.4 ± 0.4	14.2	14.6	13.4
8c	$CH(A) + H_2 + H^+$			16.59	19.7 ± 0.4	20.4		
8d	$CH(A) + 2H + H^+$			25.8	22.4 ± 0.4			20.8
				30.2	32.5 ± 0.4	32.7		35
9a	$CH(B) + H + H_2$	$B^2\Sigma^- \rightarrow X^2\Pi$	387.5	12.33	14.1 ± 0.2			
9b	$CH(B) + 3H$			16.91	15.2 ± 0.4			
9c	$CH(B) + 2H + H^+$			30.52	17.9 ± 0.4			
					20.4 ± 0.4			
10a	$CH(C) + H + H_2$	$C^2\Sigma^+ \rightarrow X^2\Pi$	314.5	13.08	15.6 ± 0.2			13.9
10b	$CH(C) + 3H$			17.66	21.2 ± 0.4			20.8
								36
11a	$CI+2H_2$	$3s^1P^o \rightarrow 2p^21S$	247.9	13.2	§			
11b	$CI+2H+H_2$			17.72	§			
11c	CI+4H			22.24	24.5 ± 0.6			24.8
								(26.2[17])
					27.3 ± 0.6			28
12	$CH^+ + H + H_2$	$B^1\Delta \rightarrow A^1\Pi$	350.2	26.25	28.4 ± 0.4			31.6
	$CH^+ + 3H$			30.75	33.1 ± 0.4			34.9

§ Threshold likely not observable due to limited count rate.

The lowest onset observed here is below 13 eV (12.6 ± 0.2 eV for $CH(A^2\Delta \rightarrow X^2\Pi)$), i.e., in the overlap with the lowest excited states. However, it is evident that in this case no CH_3 radical formation is associated with this process. Also superexcited states with excitation of two electrons of the target molecule may play a role as discussed in [24, 30] in detail. In the case of the $CH(A^2\Delta)$ fragment, we can see that the first threshold (12.6 ± 0.2 eV) approaches the calculated thermodynamic threshold for reaction 8a of 12.01 eV (see table 2; formation of H and H_2), and the second threshold with the reaction 8b as calculated from the thermodynamic data found in [47] (see table I in the supplementary material, available at stacks.iop.org/JPhysB/46/045203/mmedia). In previous studies, the experimental threshold was detected ∼2 eV above the thermodynamic threshold; in the present case, it is 0.6 eV. This difference would mean lower translational and ro-vibrational excitation of the products in the present experiment. However, we ascribe the difference in thresholds to result rather from the higher sensitivity of the present experimental setup. In the case of the excited states $CH(B^2\Sigma^-)$ and $CH(C^2\Sigma^+)$, the present experimental thresholds do not approach the theoretically predicted values so closely like in $CH(A^2\Delta)$. The difference between the dissociation limit and the thermodynamic threshold is released in the form of kinetic energies of fragments and in the internal ro-vibrational excitation of the products.

In [21], a picture of the dissociation dynamics of an initially excited methane molecule was drawn in the case of multi-photon excitation: after initial excitation a step-wise fragmentation process $CH_4 \rightarrow CH_2 \rightarrow CH + H$ was proposed by means of a simple analysis of the dissociation dynamics because the channels $CH_4 \rightarrow CH + 3H$ and $CH_4 \rightarrow CH_3 \rightarrow CH + 2H$ would not lead to ro-vibrational excitation of CH. In the case of electron excitation, the ro-vibrational states of the CH fragment are not limited to stepwise fragmentation.

The dissociation limits calculated from the thermodynamic data for the dissociation reaction $CH + H_2 + H$ of the other excited states of CH, $B^2\Sigma^-$ and $C^2\Sigma^+$, are shifted to slightly higher energies and can be found at 12.33 and 13.08 eV, respectively (see table 2). The limits for the channels with different dissociative products (8)–(11) are shifted accordingly. The lowest threshold for $CH(B^2\Sigma^-)$ observed in our measurement was 14.1 ± 0.2 eV and for the $CH(C^2\Sigma^+)$ state 15.6 ± 0.2 eV. In the case of $CH(B^2\Sigma^-)$ and $CH(C^2\Sigma^+)$, the dissociation channels 9a and 10a are accessible at the lowest threshold. Additional thresholds were obtained in $CH(B^2\Sigma^-)$ and $CH(C^2\Sigma^+)$ and correspond to the formation of three hydrogen atoms at 15.2 ± 0.4 and 21.2 ± 0.4 eV, respectively. In the case of $CH(B^2\Sigma^-)$ and $CH(C^2\Sigma^+)$ states, there most probably exists stronger energy partitioning in the products as it was in the case of the $CH(A^2\Delta)$ fragment.

We have also measured the excitation curves for Balmer lines up to (n = 9–2). In figure 6 the excitation curves of H(3–2) and H(4–2) are presented; excitation curves were also measured for the other Balmer lines up to $n = 9$ (see figure I of supplementary material available at stacks.iop.org/JPhysB/46/045203/mmedia). We were not able to measure excitation functions for $n \geqslant 10$ due to limited resolution of the optical monochromator and the low intensity of the signal. The Balmer lines H(5–2) and H(8–2) were overlapping with CH emissions bands; however, we were able to account for the CH contributions in the data analysis. From the excitation function we determined the threshold for dissociative excitation into the Balmer series. The determined values are presented in table 1. The present value for H(3–2) is shifted to a lower value (by almost 1.6 eV in comparison to Motohashi *et al* [20]). On the other hand,

the present H(4–2) value exceeds that of Motohashi *et al* by approximately 0.5 eV. The present experimental values for the first threshold are above the thermodynamic thresholds for the process:

$$e^- + CH_4 \rightarrow H(n = 3 - 9) + CH_3 + e \quad (7)$$

and below the threshold for the processes:

$$e^- + CH_4 \rightarrow CH(X) + H_2 + H^*. \quad (8)$$

The thresholds listed in table 1 lead to the following conclusions: (i) a first onset below 20 eV was observed only for H(3–2), all other Balmer lines have a threshold above 20.6 eV still associated with reaction (7); (ii) a second onset is between 25.4 and 29.1 eV. Previously Motohashi *et al* measured threshold energies for the Balmer series from H(3–2) to H(6–2) and reported a (linear) threshold increase of about 0.2–0.3 eV at each n value [20]. In the present case, the value of the first threshold increases with n. A third threshold close to 36 eV, reported for two Balmer lines [19, 20], cannot be deduced in the present measurements. This may be described by a signal/noise ratio which prevents a clear signature of the threshold. Concerning the parent molecular state it was previously suggested that vibrationally excited Rydberg states formed at electron energies above 19.5 eV (up to 24 eV) lead to dissociation into fragments including electronically excited hydrogen [20]. A list of calculated dissociation limits from thermodynamic data [47] for various combinations of fragments with excited hydrogen can be found in table 1. The lowest dissociation limit is between 16.65 ($n = 3$) and 17.978 eV ($n = 9$) and corresponds to the products H + CH_3. Dissociation reactions with simultaneous ion formation (e.g. CH_3^+, CH_2^+) can be ruled out within our investigated energy range because the thresholds observed are below the dissociation limit of these reactions [20].

The only fragment ion which shows fluorescence in the present measurements is CH^+. The observed transition at 350.2 nm can be ascribed to the $B^1\Delta \rightarrow A^1\Pi$ and we deduce a strong threshold signal at 28.4 ± 0.4 eV and the second threshold at 33.1 ± 0.4 eV (see table 2). The first value is approximately 3.2 eV lower than the first threshold of 31.6 eV reported in [19]. The second threshold is shifted to lower energies by 1.8 eV as well. Like for neutral CH, in CH^+ the lowest dissociation limit implies formation of H_2 + H and has a thermodynamic value of 26.25 eV [41]. In the case of the formation of 3H, the threshold is increased by 4.5 eV and is then above the experimental onset. It should be noted that we were not able to resolve the transitions $CH^+(A^1\Pi \rightarrow X^1\Sigma^+)$ and $CH^+(B^1\Delta \rightarrow X^1\Sigma^+)$ due to their overlap with excited states of CH and thus we were not able to determine the thresholds.

For atomic carbon, we observed fluorescence for the transition CI ($3s^1P^o \rightarrow 2p^2\,^1S$) at 247.9 nm which yields two onsets, the first one at 24.5 ± 0.6 eV and the second at 27.3 ± 0.6 eV and energetically they could be assigned to the process 11c in table 2; however, we are not able to exclude processes 11a and b as well. These onsets are in reasonable agreement with values reported in [19] for this atomic state.

Conclusion

We have carried out a comprehensive study on electron impact excitation of CH_4 utilizing an electron monochromator and detection system to monitor the photon emission of electronically excited species. In accordance with previous studies no emission of the excited parent molecule could be observed and we detected emission from the molecular (CH, and CH^+) and atomic (HI, CI) fragments. Subsequently, we have determined the corresponding threshold energies for the transitions detected. We also report threshold energies for five transitions not determined so far (H_ε(7–2), H_ζ(8–2), H_η(9–2), $CH(B^2\Sigma^- \rightarrow X^2\Pi)$). For several excitation reactions, the present data yield threshold values different from former studies (H(3–2), $CH(A^2\Delta \rightarrow X^2\Pi$ (0,0), ...), in most cases lower than in the former studies. We ascribe this to the improved resolution in the electron energy due to utilization of the electron monochromator as well as to good sensitivity and the high signal/noise ratio achieved in the present experimental system as well.

Acknowledgments

This work was supported by the Slovak Research and Development Agency, project nos APVV-0733-11 and DO7RP-0025-11, Slovak grant agency VEGA, project no 1/0379/11 and European Commission. JF acknowledges support from the COST Action CM0805 and the SNSF project no. PZ00P2-132357/1. JBM acknowledges support from the project of collaboration between Serbia and Slovakia 'Excitation and fragmentation of small biomolecules (2010–2011) and the MES RS (project no 171020). This work was supported by the European Commission under the Contracts of Association between EURATOM and the Comenius University as well as the Austrian Academy of Sciences. It was carried out within the framework of the European Fusion Development Agreement. The views and opinions expressed herein do not necessarily reflect those of the European Commission.

References

[1] Fuss M C, Muñoz A, Oller J C, Blanco F, Hubin-Franskin M-J, Almeida D, Limão-Vieira P and García G 2010 *Chem. Phys. Lett.* **486** 110–5
[2] Shemansky D E, Stewart A I F, West R A, Esposito L W, Hallett J T and Liu X 2005 *Science* **308** 978–82
[3] Huestis D L, Bougher S W, Fox J L, Galand M, Johnson R E, Moses J I and Pickering J C 2008 *Space Sci. Rev.* **139** 63–105
[4] Ajello J M, Gustin J, Stewart I, Larsen K, Esposito L, Pryor W, McClintock W, Stevens M H, Malone C P and Dziczek D 2008 *Geophys. Res. Lett.* **35** L06102
[5] Stevens M H *et al* 2011 *J. Geophys. Res.* **116** A05304
[6] Lutz B L, Owen T and Cess R D 1976 *Astrophys. J.* **203** 541–51
[7] Vuitton V, Yelle R V and McEwan M J 2007 *Icarus* **191** 722–42
[8] Hesser J E and Lutz B L 1970 *Astrophysical J.* **159** 703–18
[9] Fantz U, Meir S and the ASDEX Upgrade Team 2005 *J. Nucl. Mater.* **337–339** 1087–91

[10] Nozaki T, Unno Y, Miyazaki Y and Okazaki K 2001 *J. Phys. D: Appl. Phys.* **34** 2504
[11] Huber S E, Seebacher J, Kendl A and Reiter D 2011 *Contrib. Plasma Phys.* **51** 931–43
[12] Reiter D and Janev R K 2010 *Contrib. Plasma Phys.* **50** 986–1013
[13] Liu X and Shemansky D E 2006 *J. Geophys. Res.* **111** A04303
[14] Stano M, Matejcik S, Skalny J D and Märk T D 2003 *J. Phys. B: At. Mol. Opt. Phys.* **36** 261–71
[15] Rawat P, Prabhudesai V S, Rahman M A, Ram N B and Krishakumar E 2008 *Int. J. Mass Spect.* **277** 96–102
[16] Hoshino M, Matejcik S, Nunes Y, Ferreira da Silva F, Limao-Vieira P and Tanaka H 2011 *Int. J. Mass Spect.* **306** 51–6
[17] Pang K D, Ajello J M, Franklin B and Shemansky D E 1987 *J. Chem. Phys.* **86** 2750–64
[18] Aarts J F M, Beenakker C I M and De Heer F J 1971 *Physica* **53** 32–44
[19] Donohue D E, Schiavone J A and Freund R S 1977 *J. Chem. Phys.* **67** 769–80
[20] Motohashi K, Soshi H, Ukai M and Tsurubuchi S 1996 *Chem. Phys.* **213** 369–84
[21] Kong F, Luo Q, Xu H, Sharifi M, Song D and Chin S L 2006 *J. Chem. Phys.* **125** 133320
[22] Wu C Y R and Judge D L 1981 *J. Chem. Phys.* **75** 172–8
[23] Welch A R and Judge D L 1972 *J. Chem. Phys.* **57** 286
[24] Fukuzawa H, Odagiri T, Nakazato T, Murata M, Miyagi H and Kouchi N 2005 *J. Phys. B: At. Mol. Opt. Phys.* **38** 565
[25] Yachi K, Odagiri T, Ishikawa L, Nakazato T, Tsuchida T, Ohno N, Kitajima M and Kouchi N 2010 *J. Phys. B: At. Mol. Opt. Phys.* **43** 155208
[26] Országh J, Danko M, Ribar A and Matejcik S 2011 *Nucl. Instrum. Methods* B **279** 76–9
[27] Matuska J, Kubala D and Matejcik S 2009 *Meas. Sci. Technol.* **20** 015901
[28] Stamatovic A and Schulz G J 1970 *Rev. Sci. Instrum.* **41** 423
[29] Zubek M 1994 *J. Phys. B: At. Mol. Opt. Phys.* **27** 573–81
[30] Kramida A, Ralchenko Y, Reader J and NIST ASD Team 2012 NIST Atomic Spectra Database (ver. 5.0), [Online] National Institute of Standards and Technology, Gaithersburg, MD (http://physics.nist.gov/asd, (date last accessed 24 October 2012)
[31] Kato M, Kameta K, Odagiri T, Kouchi N and Hatano Y 2002 *J. Phys. B: At. Mol. Opt. Phys.* **35** 4383–400
[32] Möhlmann G R and de Heer F J 1979 *Chem. Phys.* **40** 157–62 and references cited therein
[33] Nishikawa S and Watanabe T 1973 *Chem. Phys. Lett.* **22** 590–4
[34] Wasowicz T J, Kivimäki A, Dampc M, Coreno M, de Simone M and Zubek M 2011 *Phys. Rev.* A **83** 033411
[35] Linert I, Lachowicz I, Wasowicz T J and Zubek M 2010 *Chem. Phys. Lett.* **498** 27–31
[36] Dampc M and Zubek M 2008 *Int. J. Mass Spectrom.* **277** 52–6
[37] Luque J and Crosley D R 1999 LIFBASE: Database and spectral simulation (version 1.5) *SRI International Report MP* 99-009
[38] Ito Y, Fujimaki A, Kobayashi K and Tokue I 1986 *Chem. Phys.* **105** 417–22
[39] Tokeshi M, Nakashima K and Ogawa T 1996 *Chem. Phys.* **203** 257–66
[40] Tokeshi M, Nakashima K and Ogawa T 1996 *Chem. Phys.* **206** 237–43
[41] Harris H H, Crowley M G and Leventhal J J 1975 *Phys. Rev. Lett.* **34** 67–70
[42] Hakalla R, Kepa R, Szajna W and Zachwieja M 2006 *Eur. Phys. J.* D **38** 481 and references therein
[43] Bettega M H F, Ferreira L G and Lima M A P 1998 *Phys. Rev.* A **57** 4987
[44] Winstead C, Sun Q, McKoy V, Lino J L S and Lima M A P 1993 *J. Chem. Phys.* **98** 2132
[45] Gil T J, Lengsfield B H, McCurdy C W and Rescigno T N 1994 *Phys. Rev.* A **49** 2551
[46] Makochekanwa C, Oguri K, Suzuki R, Ishihara T, Hoshino M, Kimura M and Tanaka H 2006 *Phys. Rev* A **74** 042704
[47] NIST Chemistry webbook, NIST Standard Reference Database Number 69 (http://webbook.nist.gov/chemistry/)